Correcting for stage error motions in radius measurements

Angela Davies and Tony L. Schmitz

Traceable radius of curvature measurements are critical for precision optics manufacturing. An optical bench measurement is repeatable and is the preferred method for low-uncertainty applications. With an optical bench, the displacement of the optic is measured as it is moved between the cat's eye and the confocal positions, each identified using a figure measuring interferometer. The translated distance is nominally the radius of curvature; however, errors in the motion of the stage add a bias to the measurement, even if the error motions are zero on average. Estimating the bias and resulting measurement uncertainty is challenging. We have developed a new mathematical definition of the radius measurand that intrinsically corrects for error motion biases and also provides a means of representing other terms such as figure error correction, wave-front aberration biases, displacement gauge calibration and their uncertainties. With this formalism, it is no long necessary to design a high-quality radius bench to carry out a precision measurement; rather a lower quality is adequate, provided that error motions are repeatable and characterized and error motion measurement uncertainties are estimated.

OCIS codes: 220.4840, 120.3180, 120.3940, 120.6650.

1. Introduction

The radius of curvature of an optical element is one of the critical parameters used to determine the performance of an optical system. Radius errors can be compensated with element respacing, but this is time-consuming, costly, and usually adds aberration to the system. To validate measurement uniformity across the industry, U.S. companies recently carried out a radius round robin of a 100 mm radius test plate.[1] The measurement divergence was of the order of 20 μm, or ~1 part in 5000, yet stated uncertainties were at the micrometer level. The divergence is larger than desired, but a precision radius measurement is susceptible to many biases, so the discrepancy is not surprising. Our goal is to improve radius metrology by enabling a detailed analysis of the measurement.

For nominally spherical components, the radius of curvature is typically defined as the radius of the best-fit sphere over the clear aperture of the lens in a least-squares sense. Many radius measurements are available, including comparison with known radius test plates, direct image formation or knife-edge test, astigmatism measurement, spherometers, autocollimator with a pentaprism, and shearing interferometers,[2,3] but the optical radius bench generally gives the lowest uncertainty. On an optical bench, the radius is measured by using a figure measuring interferometer to identify the location of the test lens at two critical positions, the confocal and the cat's eye positions [see Fig. 1(a)]. With the artifact at either of these positions, the wave front reflects back on itself and the interferometric cavity is null. A displacement gauge measures displacement as the test lens is translated between the two positions, and the recorded distance is nominally the radius of the best-fit sphere to the surface. The method is deceptively simple, however. As discussed in numerous publications, there are many sources of bias and uncertainty. Examples include identification of null at the two positions, wave-front aberrations, figure error corrections, displacement gauge reading, and errors in the translational motion between the two positions.[4–6]

The error motions are challenging because they are interrelated and convolved with the measurement. The interferometer is sensitive to the alignment of the artifact at the confocal position, but rather insensitive at the cat's eye position; therefore only large stage error motions can be observed. Figure 1(b) illustrates the consequence of a translational error

A. Davies (adavies@uncc.edu) is with the Department of Physics and Optical Science, University of North Carolina at Charlotte, 9201 University City Boulevard, Charlotte, North Carolina 28223-001. T. L. Schmitz is with the Department of Mechanical and Aerospace Engineering, University of Florida, Gainesville, Florida 32611.

Received 24 January 2005; revised manuscript received 28 April 2005; accepted 3 May 2005.

0003-6935/05/285884-10$15.00/0

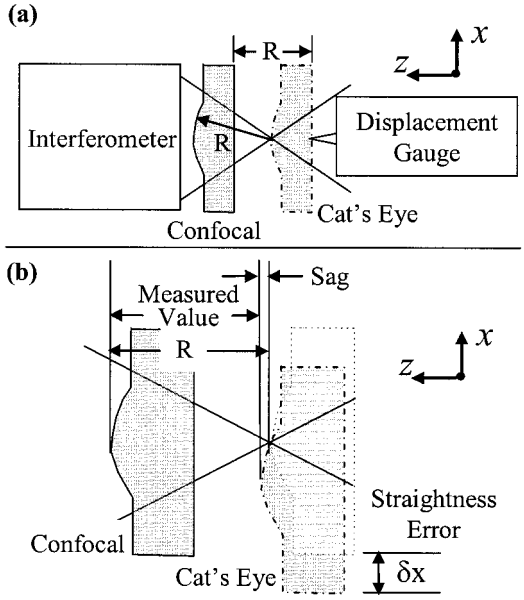

Fig. 1. Schematic of radius of curvature measurement. (a) The part is translated between the confocal and the cat's eye positions, and the measured displacement is an estimate of the radius of curvature. (b) Translation error in the x direction during the z-direction translation leads to a measured value that is less than the radius.

(straightness or squareness) in the motion. The error is exaggerated for illustration. An x-axis translation during the z motion leads to a displacement gauge reading that is less than the radius by the sag in the surface. Recent work has focused on identifying uncertainty sources, including those related to error motions, and estimating the uncertainty through a root-sum-of-the-squares (rss) combination.[5,6] This method is only approximate, however, because the measurement is not a simple linear function of the error motions. A rigorous mathematical treatment is needed to correct for the biases. Such a treatment will also enable a rigorous uncertainty evaluation.

In this paper we describe a vector-based approach to define the measurand R that corrects for errors in the translational motion. Other contributions such as wave-front aberrations and figure errors on the test lens are easily added to the model. Because the method corrects for error motions, it is no longer necessary to engineer a high-quality optical bench for precision measurements, rather error motions simply must be repeatable and well characterized. The method is based on a homogeneous transformation matrix (HTM) coordinate transformation[7] and intrinsically leads to an unbiased estimate. The method defines the radius as the magnitude of the difference between two vectors, rather than a simple projection onto the displacement gauge axis, as is currently done. One of the vectors captures the motion of the test lens, resulting from the stage error motions, and the other vector defines the focus location of the wave front exiting the interferometer. The latter can be viewed as the probe in the measurement. The HTM formalism is well known in the precision engineering community and is commonly used to analyze error motions in precision machine tools and stages.[7] This paper focuses on the theory and provides a simple example to illustrate the application.

2. Vector Definition of the Radius

A. Assumptions

To correct for errors in the motion, the errors of the optical bench must be estimated. Error motions are unwanted translations or rotations of the stage, and therefore the test lens, that occur during the displacement. In general, there are 6 degrees of freedom for motion—the stage can rotate about the three Cartesian axes (yaw, pitch, and roll), and it can experience translational errors along the axes. For general precision machine tool metrology, error motions for nominal motion along all three axes must be considered. For a radius bench, we have only nominal motion along the optical axis (z axis).

The rigid body motion of the stage can be determined through a coordinate transformation, but only if the error motions are repeatable and known. The radius uncertainty desired, the repeatability of the radius bench, and the error motion uncertainties must all be considered. For example, large error motion uncertainties will obviously lead to a larger radius measurement uncertainty, and error motions must be repeatable if the bias is to be corrected. One can divide all possibilities into three categories. The radius uncertainty goal and the repeatability of a particular radius bench will determine the category to be considered and the sophistication with which the error motions must be measured. The three categories are the following:

(i) Error motions are zero on average. This is the case with either a well-designed radius bench with error motion uncertainties larger than error motions or a poorly designed bench with error motions that vary randomly about zero (not repeatable). Surprisingly, even in this limit, the simple reading of the displacement gauge at cat's eye compared with confocal is not a good radius estimate. Most error motions, either positive or negative, lead to a gauge reading that is always less than the actual radius, which causes a bias in the measurement.[6] Our formalism intrinsically corrects for this bias.

(ii) Error motions are repeatable and increase linearly with displacement. Error motion measurement uncertainty must be less than the error motion, so the linear dependence is observable. As an example, a misalignment between the z-motion axis and the gauge axis in the x direction leads to a translational error in the x direction, δx, as the stage moves. The angle is constant, therefore δx increases linearly with displacement. This is the well-known cosine error, leading to a bias in the measurement, as illustrated in Fig. 1(b). A linear dependence for other error motions is also possible, particularly for small displacements (small radius measurements).

Table 1. Definition of Symbols and Vector Relationships

Symbols	Definition
O_s, O_r	Origins of stage and reference coordinate systems, respectively.
${}^r\mathbf{X}_p = ({}^rx_p, {}^ry_p, 0)$, ${}^s\mathbf{X}_A$	Vector defining the probe in the reference coordinate system, which is the focus of light exiting the interferometer, and the vector defining the best-fit center of the artifact in the stage coordinate system.
$\mathbf{R}$	The radius vector that defines the best-fit sphere to the surface of the test artifact over the measurement aperture.
$\mathbf{R} = {}^r\mathbf{X}_p - {}^r\mathbf{X}_A^{\mathrm{ce}}$	The radius is equal to the difference between the probe location and the center of the artifact in the reference system at cat's eye.
${}^s\mathbf{X}_A = {}^r\mathbf{X}_p + (\mathrm{d}x^{\mathrm{cf}}, \mathrm{d}y^{\mathrm{cf}}, \mathrm{d}z^{\mathrm{cf}})$	The location of the test artifact in the stage coordinate system is defined at the confocal position. At confocal, the stage and reference coordinate systems exactly overlap. The vector defining the artifact in the stage is equal to the sum of the vector defining the probe in the reference system plus uncertainties in the x, y, z artifact center due to an imperfect confocal null.
${}^r\mathbf{X}_A^{\mathrm{ce}} = {}^rT_s{}^s\mathbf{X}_A$	The coordinates of the test artifact in the reference coordinate system is given by the multiplication of the HTM and the vector defining the location of the artifact in the stage reference system.
d_{ce}	The z coordinate of the stage origin in the reference coordinate system at the cat's eye position. This is the reading of the displacement gauge after translation from confocal to cat's eye and must represent a calibrated best estimate.
$\varepsilon_x(d)$, $\varepsilon_y(d)$, $\varepsilon_z(d)$	Angular error motions (pitch, yaw, and roll), respectively, which are a function of the stage position that is defined by the gauge reading.
$\delta x(d)$, $\delta y(d)$	Straightness error motions, or displacements orthogonal to the nominal motion, which are also a function of the stage position.
${}^rT_s = f(\delta x, \delta y, \varepsilon_x, \varepsilon_y, \varepsilon_z, \mathrm{d}_{\mathrm{ce}})$	HTM used to map vectors in the stage coordinate system into the reference coordinate system. The matrix is a function of the error motions and the displacement gauge reading.
u_c	The combined standard uncertainty for R.

(iii) The error motions are repeatable nonlinear functions of the displacement. This is the generalization of case (ii). Error motions are never exactly linear—consideration of case (ii) or (iii) depends on the size of the nonlinearity compared to the measurement uncertainty. For example, the periodicity of stage components such as bearings and the lead screw inevitably lead to a periodic component to the motion. This limit must be considered in demanding radius uncertainty applications or where the instrument is poorly designed and/or fabricated.

Only rotation and/or translation that occurs during the displacement is important; consequently, the absolute position of the stage is not critical for categories (i) and (ii), but is for category (iii). The results presented here apply to categories (i) and (ii) directly, but can be used for the third category if the error motions between the absolute confocal and the cat's eye positions are known. However, this requires a well-defined stage coordinate system and a means of defining the absolute stage position. In the most demanding applications, it may also require an additional coordinate transformation that identifies the position of the stage at the measurement starting point relative to an absolute zero position.

Also, the x–y translation of the stage needed to center the test lens for the measurement must be considered. Error motions associated with x–y translation are not directly relevant, but the weight redistribution due to large x–y stage translation may significantly modify the z-axis error motions. This can be ignored when the test lens is approximately centered on the stage (and therefore the stage is in the same position for which the z-axis error motions were characterized). In contrast, radius measurements of microlens arrays that are fabricated in large numbers over large areas lead to significant x–y translation of the stage. In this case, the z-axis error motions should be characterized for a range of x–y stage positions.

Consideration of radius measurements falling in categories (i) or (ii) simplifies the final equation considerably, and provides a reasonable starting point for an introduction to the method. Even so, the calculation is complicated and involves many variables. A summary of the symbols and key relationships is provided in Table 1.

B. Defining the Coordinate Systems

A vector relationship describing R requires the definition of two coordinate systems—a system fixed to the stage and one fixed to the probe that completes the metrology loop. A spherical test artifact will be used for the diagrams and discussion to follow. The test artifact is rigidly attached to the stage and there is a unique vector that defines its location, which we take to be the center of curvature. The radius measurement is based on artifact positions at which the converging interferometer beam reflects back onto

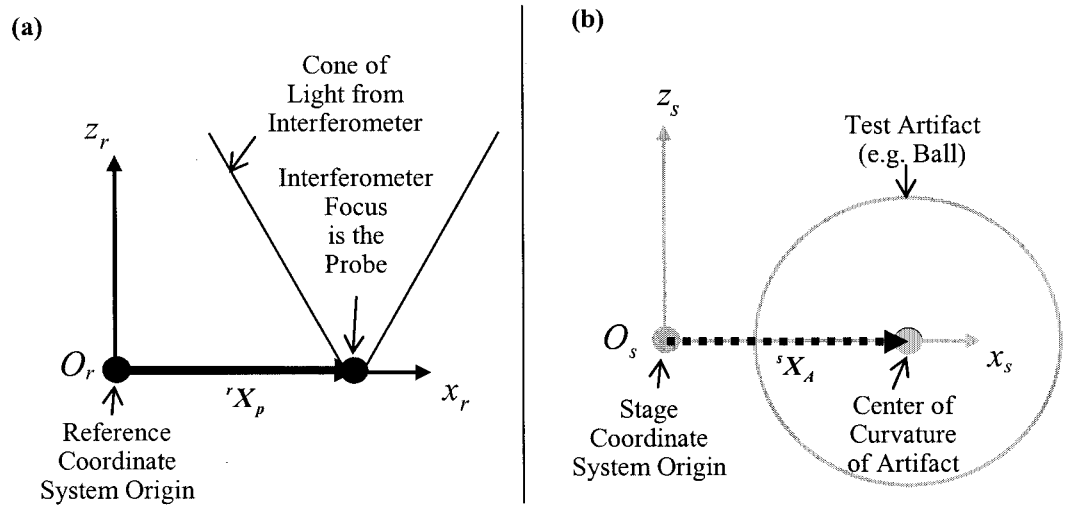

Fig. 2. (a) Schematic of reference coordinate system, which is fixed in the laboratory reference frame. The focus of the test beam exiting the interferometer is considered the probe. The vector shown is the location of the probe in the reference coordinate system, $^r\mathbf{X}_p$. (b) Schematic of the stage coordinate system. The test artifact (a ball in this case) is fixed in this frame and the location is defined by the vector $^s\mathbf{X}_A$, which locates the center of curvature of the artifact in the stage coordinate system. The stage coordinate system is taken to overlap with the reference coordinate system at the confocal position (the condition shown). Possible biases and uncertainties from this assumption are discussed in the text.

itself; therefore the location of the beam focus is also critical. If we consider the beam focus as a probe, then the confocal corresponds to the position where the probe is coincident with the center of curvature of the artifact and the cat's eye to the position where the probe is coincident with the surface. Rigorously, this definition breaks down when aberrations and diffraction are considered. More exactly, the probe location is best defined as the center of curvature of the wave front where the wave-front curvature matches the curvature of a best-fit sphere over the test part subaperture sampled at the confocal. The probe is fixed in the laboratory frame, and we will define a reference coordinate system also fixed in the laboratory frame. We define the z axis of the reference frame as the axis of the displacement gauge. Because we are considering categories (i) and (ii) where only the change in the error motions is needed, the absolute z coordinate of the probe or artifact is not important and can be set to zero. The two coordinate systems are shown in Fig. 2. An Abbe offset may be present on the radius bench and this is represented in the model by an x–y offset between the displacement gauge axis and the probe. An Abbe error occurs when the gauge axis is offset from the probe and angular motion error occurs during the translation.[7,8]

There are three axes involved in the measurement and it is worth emphasizing the role played by each. The three axes are the gauge axis, the motion axis, and the optical axis. The gauge axis is the one-dimensional line along which the gauge reading represents the displacement. For example, with a displacement measuring interferometer (DMI) as the gauge, the gauge axis would be the optical axis of the DMI.[8] This axis is defined either in the gauge installation or a gauge calibration procedure. The motion axis is the line in space traced out by an identified origin on the stage as the stage is displaced. Ideally the gauge axis and the motion are parallel and coincident to minimize cosine and Abbe errors. The optical axis is the line through the center of the optical beam in the interferometer. Interestingly, the orientation of this axis relative to the other two has only a small effect on the measurement and is discussed in more detail in Subsection 2.G.

C. Vector Definition of *R*

To introduce our formalism, we begin with a schematic of the radius measurement for perfect (and unrealistic) z motion [Fig. 3(a)]. The starting point should always be the confocal position because the x–y alignment of the test artifact can only be assessed here—the wave front that retroreflects at cat's eye is insensitive to the local slope and therefore insensitive to the x–y location of the beam relative to the artifact apex. The displacement gauge is zeroed at confocal. Without error motions, the stage translates perfectly to cat's eye and the gauge reading (which is the z coordinate of the stage in the reference frame) is the value of the radius.

Because we restrict our analysis to categories (i) and (ii) where absolute z and x–y coordinates are not critical (assuming that the error motions for the z-axis translation have been determined for the current x–y stage position), we can define the stage coordinate system to overlap with the reference system at the confocal. This choice then defines the location of the artifact in the stage coordinate system. Namely, the vectors $^r\mathbf{X}_p$ and $^s\mathbf{X}_A$ are equal at this point, but only up to the ability to null the interferometer at confocal. The superscript to the left of a vector

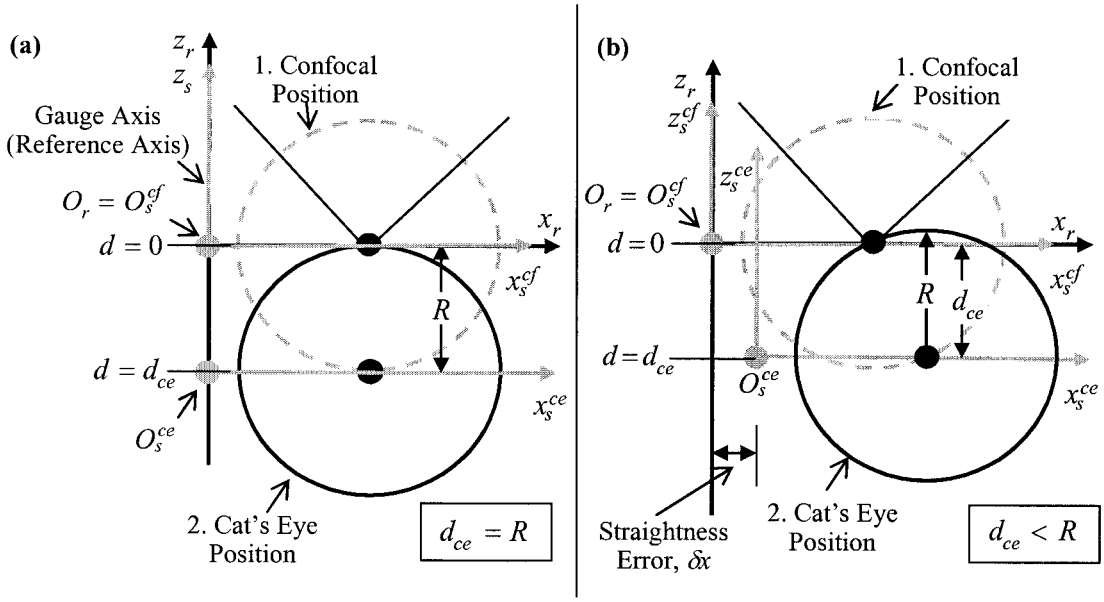

Fig. 3. (a) Radius measurement with no error motions and with the motion axis parallel to the gauge axis (the reference axis). The gauge axis may be offset from the optical axis to capture Abbe errors. At the confocal position the z-axis coordinate of the probe in the reference frame and the z-axis coordinate of the artifact in the stage frame are both zero. The stage and the origins overlap at this position and the displacement gauge is zeroed. In the absence of error motions, the displacement gauge reading at cat's eye is equal to the radius of the artifact. (b) Same conditions as in (a), but x-axis straightness is added. Error motions now cause the artifact to translate to the right; therefore the cat's eye reflection occurs away from the apex of the artifact. The displacement gauge, having been zeroed at confocal, now reads a value at cat's eye that is less than the true radius.

will denote the reference frame in which the vector is defined. This gives us

$$ {}^{s}\mathbf{X}_A = {}^{r}\mathbf{X}_p + (\mathrm{d}x^{\mathrm{cf}},\ \mathrm{d}y^{\mathrm{cf}},\ \mathrm{d}z^{\mathrm{cf}}). \tag{1}$$

Again, the x–y coordinates of the probe are allowed to be nonzero, as this is necessary to represent Abbe errors.

The effect of error motions can be immediately appreciated from Fig. 3(b), which depicts straightness error during the measurement. The measurement still begins at confocal where the stage and reference frames are defined to overlap and the gauge is zeroed. Now the translation to cat's eye causes the artifact to shift to the right. The null at cat's eye is still the location where the probe coincides with the artifact surface, but this is no longer at the apex of the artifact. The gauge reads the z coordinate of the stage in the reference frame (the displacement along the gauge's axis), which is smaller than the artifact radius.

Rather than approximately define the radius as only the projection of the artifact position onto the gauge axis (reference z axis), it can be defined exactly with the appropriate vectors, as shown in Fig. 4. If the location of the artifact at cat's eye is known, the vector defining the radius is given by

$$\mathbf{R} = {}^{r}\mathbf{X}_p - {}^{r}\mathbf{X}_A{}^{\mathrm{ce}}, \tag{2}$$

and the magnitude of $\mathbf{R}$ is given by

$$R^2 = |\mathbf{R}|^2 = |{}^{r}\mathbf{X}_p - {}^{r}\mathbf{X}_A{}^{\mathrm{ce}}|^2. \tag{3}$$

The superscript to the right indicates the measure-

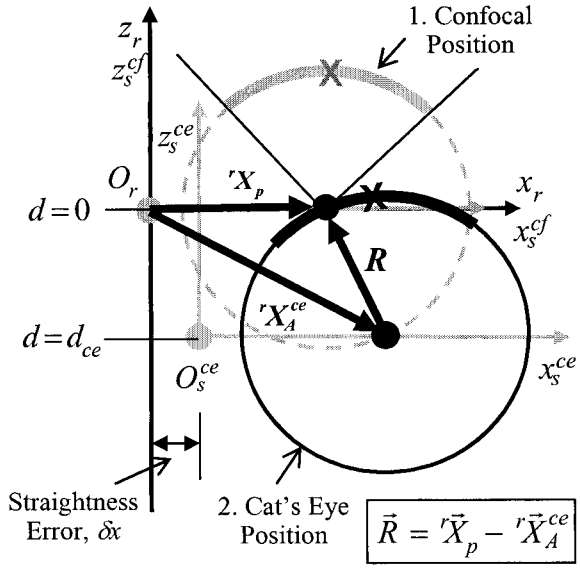

Fig. 4. Same conditions as in Fig. 3, but showing the correct definition of the measurand R, which is in terms of the vectors defining the location of the probe and the center of curvature of the artifact in the reference coordinate system. The subaperture of the sphere measured at confocal is highlighted with a heavy gray curve and an X is included to indicate the center of the aperture. The same aperture and center location are indicated at cat's eye with a heavy black curve and an X.

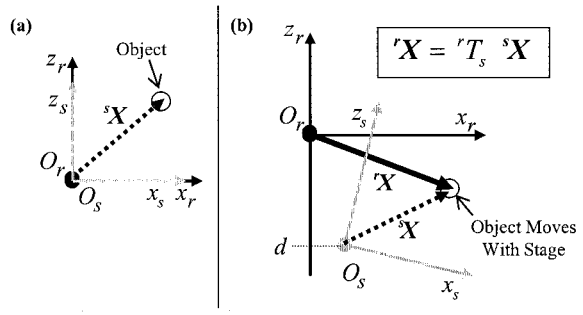

Fig. 5. Schematic of a HTM characterization of nominal z motion of a stage relative to a fixed reference coordinate system. (a) The vector ${}^s\mathbf{X}$ locates an object fixed in the stage reference frame. (b) The stage is moved to a position d along the reference z axis and the motion can be described by a HTM ${}^rT_s$. Error motion measurements determine the elements of the HTM, and the z axis of the reference coordinate system is the displacement gauge axis so the gauge reads a displacement of d. The location of the object on the stage is located at ${}^r\mathbf{X} \simeq {}^rT_s{}^s\mathbf{X}$ in the reference coordinate system after the motion.

ment position at which the vector is defined. Note that the position of the artifact must be known in the reference coordinate system, ${}^r\mathbf{X}_A{}^{ce}$.

D. Describing the Motion with a Homogeneous Transformation Matrix

Equation (3) defines the measurand, but knowledge of the error motions is needed to determine ${}^r\mathbf{X}_A{}^{ce}$. We must map the coordinates of the artifact at the new stage position back to the reference coordinate system. This is best done with a HTM.[7] A HTM is a 4 $\times$ 4 matrix that captures the rotation and/or translation of one coordinate system relative to another and allows a vector in one system to be mapped to the other. In general, matrices that represent rotation about orthogonal axes do not commute, but they do in the limit of small rotations. Small rotations are reasonable assumptions for a well-designed radius bench, and in this limit a general HTM for a nominal displacement of d along the z axis is given by[7]

$$ {}^rT_s = \begin{bmatrix} 1 & -\varepsilon_z & \varepsilon_y & \delta x \\ \varepsilon_z & 1 & -\varepsilon_x & \delta y \\ -\varepsilon_y & \varepsilon_x & 1 & d \\ 0 & 0 & 0 & 1 \end{bmatrix}, \tag{4} $$

where the variables are as defined in Table 1, and the explicit reference to the dependence of the error motions on d has been dropped for convenience. The fourth row of the HTM allows the rotation and translation to be incorporated into the same matrix and can be used to modify scaling. The error motions may be proportional to the gauge reading, d [case (ii)], with the error motions equal to zero for zero displacement. Therefore terms in the matrix must represent the total angular errors ε_x, ε_y, ε_z and final x–y displacement errors δx and δy that the stage experiences during the motion from confocal to cat's eye. Note

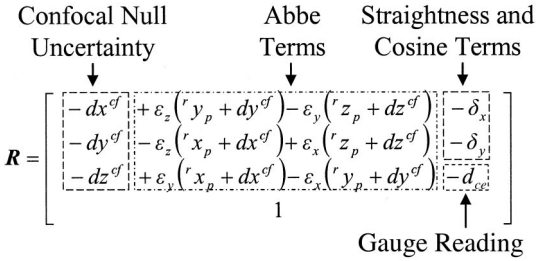

Fig. 6. Components of vector $\mathbf{R}$ that define the radius of the test artifact. The magnitude of this vector is the radius measurand R. See text for a discussion of the terms.

that the effect of cosine error and straightness error both combine and lead to overall values of δx and δy.

The coordinate mapping is illustrated in Fig. 5. Figure 5(a) shows the overlap between a stage and a reference coordinate system. The vector ${}^s\mathbf{X}$ defines the location of an object in the stage coordinate system, and this is also the vector that defines the object location in the reference frame before the motion [part (a)]. After the rigid body motion of the stage, the object has moved in the reference frame, while remaining fixed in the stage frame. The new coordinates in the reference frame are given by ${}^r\mathbf{X} = {}^rT_s{}^s\mathbf{X}$. This equation becomes

$$ \begin{bmatrix} {}^rx \\ {}^ry \\ {}^rz \\ 1 \end{bmatrix} = \begin{bmatrix} 1 & -\varepsilon_z & \varepsilon_y & \delta x \\ \varepsilon_z & 1 & -\varepsilon_x & \delta y \\ -\varepsilon_y & \varepsilon_x & 1 & d \\ 0 & 0 & 0 & 1 \end{bmatrix} \begin{bmatrix} {}^sx \\ {}^sy \\ {}^sz \\ 1 \end{bmatrix}. \tag{5} $$

The entry in the ${}^s\mathbf{X}$ vector is set to one to provide unity scaling.

We can apply Eq. (3) to our problem by populating ${}^rT_s$ with the estimated stage error motions and by defining the center of the artifact as the object fixed in the stage frame.

E. Equation that Defines the Measurand R

Multiplying the vector that defines the artifact location in the stage frame by the HTM determines the location in the reference frame, namely,

$$ {}^r\mathbf{X}_A{}^{ce} \equiv {}^rT_s{}^s\mathbf{X}_A. \tag{6} $$

After substituting Eqs. (1) and (6) into Eq. (2) we see that R is defined by

$$ \mathbf{R} \equiv {}^r\mathbf{X}_p = {}^rT_s \begin{bmatrix} {}^rx_p + \mathrm{d}x^{\mathrm{cf}} \\ {}^ry_p + \mathrm{d}y^{\mathrm{cf}} \\ \mathrm{d}z^{\mathrm{cf}} \\ 1 \end{bmatrix}. \tag{7} $$

With substitution of Eq. (4) for the HTM, we can write out the components of $\mathbf{R}$. This is shown in Fig. 6. We need to calculate the magnitude of $\mathbf{R}$, which involves squaring and summing the three compo-

nents. The algebra is very involved and it is best to verify the results with a symbolic programming language such as Maple. We find that

$$R = \left[\begin{array}{l} d_{\mathrm{ce}}{}^2 + \delta_x{}^2 + \delta_y{}^2 + (\mathrm{d}x^{\mathrm{cf}})^2 + (\mathrm{d}y^{\mathrm{cf}})^2 + (\mathrm{d}z^{\mathrm{cf}})^2 + 2\mathrm{d}x^{\mathrm{cf}}\ \delta x + 2\mathrm{d}y^{\mathrm{cf}}\ \delta y + 2\mathrm{d}z^{\mathrm{cf}} d_{\mathrm{ce}} \\ + \varepsilon_z{}^2\left[{}^r y_p{}^2 + 2{}^r y_p \mathrm{d}y^{\mathrm{cf}} + (\mathrm{d}y^{\mathrm{cf}})^2\right] + \varepsilon_z{}^2\left[{}^r x_p{}^2 + 2{}^r x_p \mathrm{d}x^{\mathrm{cf}} + (\mathrm{d}x^{\mathrm{cf}})^2\right] \\ + \varepsilon_y{}^2\left[{}^r x_p{}^2 + 2{}^r x_p \mathrm{d}x^{\mathrm{cf}} + (\mathrm{d}x^{\mathrm{cf}})^2\right] + \varepsilon_x{}^2\left[{}^r y_p{}^2 + 2{}^r y_p \mathrm{d}y^{\mathrm{cf}} + (\mathrm{d}x^{\mathrm{cf}})^2\right] \\ + \varepsilon_x{}^2(\mathrm{d}z^{\mathrm{cf}})^2 + \varepsilon_y{}^2(\mathrm{d}z^{\mathrm{cf}})^2 \\ + 2\varepsilon_z \delta_y{}^r x_p - 2\varepsilon_z \delta_x{}^r y_p + 2\varepsilon_x{}^r y_p d_{\mathrm{ce}} - 2\varepsilon_y{}^r x_p\, d_{\mathrm{ce}} + 2\mathrm{d}y^{\mathrm{cf}} \varepsilon_x d_{\mathrm{ce}} - 2\mathrm{d}x^{\mathrm{cf}} \varepsilon_y d_{\mathrm{ce}} \\ + 2\mathrm{d}y^{\mathrm{cf}} \varepsilon_z({}^r x_p - \delta_x) - 2\mathrm{d}x^{\mathrm{cf}} \varepsilon_z({}^r y_p - \delta_y) + 2\mathrm{d}z^{\mathrm{cf}} \varepsilon_x({}^r y_p - \delta_y) \\ - 2\mathrm{d}z^{\mathrm{cf}} \varepsilon_y({}^r x_p - \delta_x) - 2\varepsilon_x \varepsilon_y({}^r x_p {}^r y_p + {}^r x_p \mathrm{d}y^{\mathrm{cf}} + {}^r y_p \mathrm{d}x^{\mathrm{cf}} + \mathrm{d}x^{\mathrm{cf}} \mathrm{d}y^{\mathrm{cf}}) \\ - 2\varepsilon_x \varepsilon_z({}^r x_p \mathrm{d}z^{\mathrm{cf}} + \mathrm{d}x^{\mathrm{cf}} \mathrm{d}z^{\mathrm{cf}}) - 2\varepsilon_y \varepsilon_z({}^r y_p \mathrm{d}z^{\mathrm{cf}} + \mathrm{d}y^{\mathrm{cf}} \mathrm{d}z^{\mathrm{cf}}) \end{array} \right]^{1/2}, \tag{8}$$

where all the variables are as defined in Table 1.

F. Interpretation of Terms

The components of **R** shown in Fig. 6 are arranged to illustrate a connection to physical processes. Note that the largest term, by far, should be the gauge reading at cat's eye, d_{ce}. The gauge reading is the correct radius if there are no misalignments or errors in the motion. The grouped terms on the far left represent misalignment at the confocal starting position. The group in the middle is a combination of angular motion errors and probe offset terms. These represent Abbe-like errors. The terms on the right describe pure translation of either unintentional x–y motion or the intentional motion along the gauge axis (z). The x–y translation may be due to a misalignment between the motion axis and the gauge axis (cosine error) and/or straightness errors. One can consider nonzero error motions one at a time to see that the magnitude of **R** does indeed yield a nonbiased estimate of the radius. For example, with x translation error δx, the radius would be given by the hypotenuse of the triangle with sides d_{ce} and δx (see Fig. 4).

Equation (8) shows that the expanded expression for the magnitude of **R** has many terms, most of which are combinations of error motions. The effect of each error motion is not independent, rather they are interrelated and convolved with the measurement. It would be extremely difficult to predict the presence of all terms in Eq. (8) with a simple geometric analysis. It is interesting to note that the HTM vector approach automatically corrects for a subtle intrinsic bias in the measurement. Consider that x–y misalignment errors at confocal and x–y translation errors lead to a gauge reading that is always too small. Consequently, even if x–y errors are zero on average, the distribution of gauge values will be one sided for these random variables. Therefore the mean of the gauge distribution is not a good radius estimate—it is biased, shifted to smaller values. This has been pointed out in the literature (specifically in the context of cosine error), and it was shown that the bias can be corrected by adding the variance of the x–y translation errors to the square of the gauge reading.[6,8] The addition of these variances appears directly in Eq. (8), providing the same bias correction. Our analysis also shows that the x–y misalignment at confocal also leads to a bias that must be corrected. To our knowledge this has not been mentioned in the literature.

The appearance of the $(\mathrm{d}z^{\mathrm{cf}})^2$ term might at first appear to add an erroneous bias correction. With zero average z misalignment at confocal (the expectation of $\mathrm{d}z^{\mathrm{cf}}$ equal to zero), the gauge distribution should be double sided for changes in $\mathrm{d}z^{\mathrm{cf}}$. In other words, the gauge can read a larger or smaller value than R. In this case, the mean value of the gauge reading is a good estimate of R; consequently the appearance of the $(\mathrm{d}z^{\mathrm{cf}})^2$ term seems to correct for a bias that should not be present. A statistical analysis of Eq. (8) shows that the $(\mathrm{d}z^{\mathrm{cf}})^2$ term is balanced by the cross term $2dz^{\mathrm{cf}} d_{\mathrm{ce}}$, thus the distribution for R predicted by Eq. (8) is correctly double sided for the random variable $\mathrm{d}z^{\mathrm{cf}}$.

G. Additional Bias Corrections and Uncertainty Sources to Consider

We have considered misalignment at confocal and errors in the motion to derive Eq. (8), but there are other mechanisms that can introduce a bias and uncertainty in a radius measurement.[4–6] All additional mechanisms can be viewed as introducing a bias in the identification of null at the confocal and/or cat's eye positions. Our model assumes that the gauge is zeroed at the confocal null position, and the best estimate of the displacement along the gauge axis to reach the cat's eye null, d_{ce}, is needed. Factors that add a bias to the identification of null at confocal can

be treated as bias corrections to dz^{cf}, and similarly bias corrections can be added to d_{ce}. Examples of mechanisms to consider include (i) residual misalignment corrections at confocal and cat's eye; (ii) figure error correction; (iii) wave-front aberrations; (iv) diffraction effects; (v) temperature effects, including possible temperature changes of the artifact during the displacement from confocal to cat's eye and the influence of temperature on the gauge reading; (vi) distortions in the imaging optics; (vii) interferometer wavelength uncertainty; and (viii) phase measurement errors. These uncertainty sources have been discussed in detail elsewhere.[5] Thus dz^{cf} can be considered a simple sum of bias corrections, $dz^{cf} = 0 + \delta_i + \delta_{iii} + \delta_{iv} + \ldots$ as appropriate, and similarly d_{ce} can be considered as $d_{ce} = d_{gauge} + \delta_i + \delta_{ii} + \ldots$ as appropriate. The uncertainties for dz^{cf} and d_{ce} are needed to estimate the final combined uncertainty for the radius and these should be determined through error propagation of the above two expressions for dz^{cf} and d_{ce}, which will be a simple rss treatment. For example, in most measurements both dz^{cf} and d_{ce} will need a bias correction due to residual misalignment (δ_i), and the uncertainty in these corrections will be one of the terms determining the combined uncertainties for dz^{cf} and d_{ce}. The figure error correction can add a bias to d_{ce} and the uncertainty in this correction will be another term determining a combined uncertainty for d_{ce}.

Note that the alignment of the optical axis does not directly appear in our HTM treatment. Consider the heavy gray and black curves in Fig. 4. These regions emphasize the subaperture of the test artifact measured at the confocal position and the X indicates the center of the aperture. The optical axis is the line intersecting the X at confocal and the probe location. If the optical axis is misaligned relative to the reference axis then the sampled aperture at confocal is rotated compared with the subaperture shown in Fig. 4. If the test artifact is a perfect sphere, then the magnitude of the resulting radius vector will still be correct—the length of any line traced from a sphere's center to the surface is the radius. However, figure error corrections must be taken into account for a realistic test artifact surface. The magnitude of the figure error correction comes from knowledge of the figure error measurement at the confocal position and knowledge of the probe location at the cat's eye position. The connection between the camera coordinate system and the part coordinate system at confocal requires knowledge of the optical axis alignment, and the probe location at cat's eye requires knowledge of the error motions. In principle, the HTM could be inverted to determine the probe location on the part at cat's eye, but this level of treatment is likely not necessary. The figure error correction will be dominated by low-spatial-frequency errors on the test artifact surface for smooth optics and small optical axis misalignments, and error motions will not lead to figure error corrections significantly different from that predicted for perfect alignment and motion.

3. Monte Carlo Simulation to Estimate *R* and the Measurement Uncertainty

Our estimate of the radius will be the expected value (the expectation value) of Eq. (8). One might naïvely substitute the expected values of all parameters into Eq. (8) (such as the expectation value of the gauge reading $\langle d \rangle$, angular error motions $\langle \varepsilon_x \rangle$, $\langle \varepsilon_y \rangle$, $\langle \varepsilon_z \rangle$, etc.) and evaluate the expression. However, this is incorrect. Direct substitution of expectation values into any measurand equation is correct only if the equation is a linear combination of the random variables, which Eq. (8) clearly is not.[9] Rigorously, the expectation value of an arbitrary function is equal to the function [e.g., Eq. (8)] multiplied by the probability distributions for all random variables, integrated over all possible values of the random variables[9] (assuming random variables are uncorrelated). Only if the function is linear does this simplify and equate to a direct substitution of expectation values. The expectation value integral can be quite complicated and difficult to calculate for a general nonlinear function. Such is definitely the case here.

The appearance of the $(dz^{cf})^2$ term discussed above immediately illustrates that direct substitution of expectation values into Eq. (8) is incorrect. Consider that all random variables in Eq. (8) are exactly zero and let only the misalignment along the z axis at confocal dz^{cf} vary randomly. Further assume that the expectation value of dz^{cf} is zero, but of course the variance is not. In this case, the expectation value of the gauge reading at cat's eye d_{ce} alone should be a good estimate of the radius. But direct substitution of expected values into Eq. (8) shows this is not the case. The expectation value of the cross term $2dz^{cf}d_{ce}$ is zero, but the expectation value of $(dz^{cf})^2$ is nonzero, which adds to the expectation of $(d_{ce})^2$. After taking the square root, the result will clearly be greater than the gauge reading and therefore not a good estimate of the radius.

When the measurand equation is complicated and nonlinear, a Monte Carlo simulation is a reasonable approach to estimate the expectation value. By simply calculating Eq. (8) for a collection of randomly chosen variables, the resulting distribution of R values captures what is expected experimentally, and the mean of the distribution will be a good estimate of the expectation value. An estimate of the probability distribution for each variable is needed to carry out the Monte Carlo simulation, including the shape of the distribution (usually Gaussian), the mean, and the width. This information comes from the assessment of the error motions and all the uncertainty sources considered.

The Monte Carlo simulation also provides an estimate of the uncertainty. The width of the simulated R distribution reflects the expected variation in R

Table 2. Parameter Values Used for the Examples

Parameter a_i	Expectation of Parameter $\langle a_i \rangle$	Estimated Uncertainty in Parameter $\langle \Delta a_i \rangle = u_{a_i}$
${}^{r}x_p$, ${}^{r}y_p$	0	2 mm
ε_x, ε_y, ε_z	0	10^{-5} rad
δx, δy	0	0.0013 mm
dx^{cf}, dy^{cf}	0	0.006 mm
dz^{cf}	0	0.003 mm
d_{ce}	0.408 mm	0.006 mm
R	0.408 mm	u_c = 0.007 mm

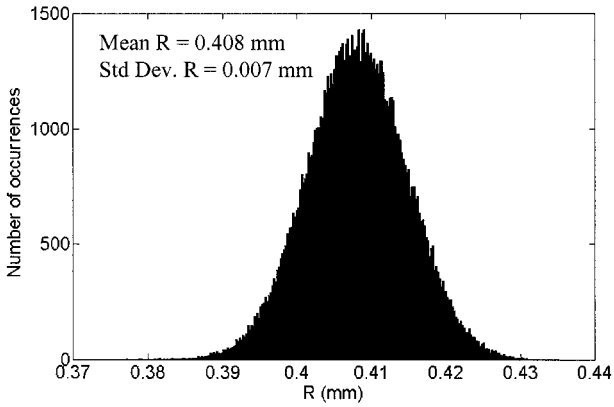

Fig. 7. Histogram of the Monte Carlo results for the radius measurement illustration discussed in the text. Random values drawn from Gaussian distributions were used for the variables in Table 2 to calculate the radius measurand as defined by Eq. (8) (100,000 iterations).

taking all uncertainty sources into account. The standard deviation will be a good estimate of the combined standard uncertainty u_c (Refs. 10 and 11) if all uncertainty sources have been taken into account. For example, the distributions used for dz^{cf} and d_{ce} should have a mean that is corrected for all suspected biases and a width that reflects the combined uncertainty for each. Their combined uncertainties should include all uncertainty contributions that affect the determination of null at the two locations.

4. Illustration with an Example

The complexity of evaluating the expectation value of Eq. (8) and estimating the uncertainty will be system dependent, and it is therefore not possible to define reduced equations that apply in all instances. In this section, we apply the new analysis to a radius measurement of a microsphere on a microinterferometer as an example.

Table 2 summarizes the expectation values and uncertainties in our example. The error motions are zero on average and the estimated uncertainties are shown. The methods by which error motions were measured and uncertainties estimated are described elsewhere.[12] Our displacement gauge is a linear voltage displacement transducer (LVDT), and the final analysis shows that the dominant uncertainty components are the z positions of the stage at confocal and cat's eye, which are reflected in the uncertainties $u_{d_{ce}}$ and $u_{dz^{ce}}$. Bias corrections to dz^{cf} and d_{ce} are small in our case compared with the final uncertainties and are therefore negligible. The Monte Carlo analysis performed with Eq. (8) and the values in Table 2 yielded a best estimate for the radius as 0.408 mm and a combined uncertainty of 0.007 mm, representing 1.7%. The histogram of the Monte Carlo results is shown in Fig. 7. The combined uncertainty is dominated by the repeatability of the measurement and the calibration of the LVDT. Note that the LVDT reading at cat's eye, having been zeroed at confocal, is also 0.408 mm. This indicates that the bias correction terms in Eq. (8) are small compared with the measurement uncertainty for this example. The uncertainty in d_{ce} is 0.006 mm and the final combined uncertainty in R is 0.007 mm. The combined uncertainty is larger because of the uncertainty in the z position at confocal. For systems with better repeatability and lower gauge calibration uncertainties, the biases and other uncertainty components will become more significant.

5. Summary

We have developed a rigorous mathematical definition of the radius for an optical bench radius measurement that intrinsically corrects for errors in the motion during the measurement. The method is based on a vector equation and a homogeneous transformation matrix (HTM) to track the position of the artifact during the translation from confocal to cat's eye. The final equation directly captures the effect of all error motions and provides the structure for mathematically incorporating all uncertainty sources. A final estimate of the radius from a measurement is best accomplished through a Monte Carlo simulation into which estimates of all error motions, their uncertainties, and all other uncertainty estimates must be incorporated. We illustrate the application of the new method with a simple example.

The authors thank S. Smith, R. Hocken, and M. Davies at the University of North Carolina at Charlotte for helpful discussions about homogeneous transform matrices and coordinate mapping; T. Estler at the National Institute of Standards and Technology (NIST) for helpful discussions on uncertainty analysis; and C. J. Evans at Zygo Corporation for helpful discussions on uncertainty components in radius measurements. This material is based on research supported by NIST and the National Science Foundation under grant 0348142. Any opinions, findings, and conclusions or recommendations expressed in this material are those of the authors and do not necessarily reflect the views of the National Science Foundation.

References and Notes

1. Sponsored by R. Plympton, Optimax Systems, Inc., Ontario, N.Y.

2. D. Malacara, *Optical Shop Testing* (Wiley, 1992).
3. M. Murty and R. Shukla, "Measurements of long radius of curvature," Opt. Eng. **22,** 231–235 (1983).
4. L. Selberg, "Radius measurement by interferometry," Opt. Eng. **31,** 1961–1966 (1992).
5. T. Schmitz, C. J. Evans, and A. Davies, "An investigation of uncertainties limiting radius measurement performance," in *Proceedings of ASPE Spring Topical Meeting* (American Society of Precision Engineering, 2000), p. 27.
6. T. Schmitz, A. Davies, and C. J. Evans, "Uncertainties in interferometric measurements of radius of curvature," in *Optical Manufacturing and Testing IV*, H. P. Stahl, ed., Proc. SPIE **4451,** 432–447 (2001).
7. A. Slocum, *Precision Machine Design* (Prentice-Hall, 1992).
8. T. Schmitz, C. J. Evans, A. Davies, and W. T. Estler, "Displacement uncertainty in interferometric radius measurements," Ann. CIRP **51/1,** 451–454 (2002).
9. P. R. Bevington and D. K. Robinson, eds., *Data Reduction and Error Analysis for the Physical Sciences*, 2nd ed. (WCB/McGraw-Hill, 1992).
10. "Guide to the expression of uncertainty in measurement" (International Organization for Standardization, 1995).
11. B. Taylor and C. Kuyatt, "Guidelines for evaluating and expressing the uncertainty of NIST measurement results," NIST Tech. Note 1297 (National Institute of Standards and Technology, 1994).
12. D. Karodkar, N. Gardner, B. Bergner, and A. Davies, "Traceable radius of curvature measurements on a microinterferometer," in *Optical Manufacturing and Testing IV*, H. P. Stahl, ed. Proc. SPIE **5180,** 261–273 (2003).